How Porous Nanofibers Have Enhanced the Engineering of Advanced Materials: A Review

Niloufar Sabetzadeh and Ali Akbar Gharehaghaji

Abstract— **Nanofibers are one-dimensional nanomaterials with a superfine diameter and many potential applications due to their desirable characteristics such as small diameter, high surface area, high flexibility, high porosity, and special mechanical properties. In the recent years, porous nanofibers have been the subject of considerable research works in a wide range of applications owing to high surface area to volume ratios and high porosity ratio. Combination of superfine diameter and porosity in porous nanofibers represent an emergent class of nanoporous materials with maximum conceivable specific surface area, high pores volume and extreme adsorption capacity that could lead to improvement in many applications such as tissue engineering, catalysts, sensors, batteries, energy storage, adsorption/separation, filtration, medical applications, solar cells, superhydrophobic surfaces, supercapacitors, and conductors. The present review focuses on the current progresses in the fabrication mechanisms and characterization methods of porous nanofibers. In addition, some application capabilities of porous nanofibers that were reported in literature are discussed and an outline of future trends is presented.**

*Keywords***: electrospinning, nanofibers, porosity**

I. INTRODUCTION

A. Nanofibers

Nanotechnology refers to the science and manufacturing of materials, structures and devices which at least one of their dimensions is 100 nm or lower [1]. Nano-scaled materials can be classified as zero-dimensional, one-dimensional, two-dimensional, and three-dimensional materials. This cataloguing is based on the number of dimensions, which are not confined to the nanoscale range [2]. In recent years, nanomaterials have attracted great attention due to their superior physical and mechanical properties, large surface area and many active surface sites [3,4]. Among different nanomaterials, nanofibers have been extensively applied in industry because of their easy fabrication procedures, compared to other nanomaterials, and their many potential applications in various fields [3].

Nanofibers, known as superfine fibers, have a diameter smaller than 500 nanometers and an aspect ratio (length to diameter ratio) of at least 100:1, and are classified as one-dimensional (1-D) nanomaterials [1,5]. When the diameter

of polymer fibers is reduced from micrometers to nanometers, some desirable characteristics such as surface area, flexibility, functionalities and mechanical performance improves significantly [6,7]. According to applicable properties of nanofibers, they have many prospective applications in areas as diverse as filtration, sensors, drug delivery, biomedical, protective clothing, catalysis, energy storage and generation, etc. [8].

So far, many different procedures have been developed to produce polymeric nanofibers, such as electrospinning, bubbfil spinning, melt blowing, phase separation, self-assembly and template synthesis [6,9-11]. For instance, bubbfil spinning as the most advanced and promising technology for mass production of nanofibers, uses bubbles of polymer solutions or melts or films for fabricating nanofibers using either air blowing and/or electric force. Sometimes, magnetic force or mechanical force have been used a swell [12,13]. Dyeing nanofibers, hierarchical nanofibers and heat-resisting nanofibers are produced by bubbfil spinning and this method has many applications in different areas such as wound dressing and filtration [14-18]

Electrospinning is a very simple, convenient and the most straightforward technique that has been widely employed to produce fibers with a diameter range from nanometers to a few micrometers. Compared to other processes, the most substantial advantage of electrospinning relies on its relatively easy and inexpensive procedure in fabrication of different kinds of nanofibers with various forms such as interconnected fibrous layers, aligned nanofibers, and twisted nanofibrous structures (nanofiber yarns). More than 100 different types of natural and synthetic polymers have been electrospun with desirable properties for a wide range of applications [19-26].

A typical electrospinning system consists of an electrical generator as a high voltage supply, a syringe with a capillary tip, containing a polymer solution, and a metal collector, which are shown in Fig. 1 [3]. During the electrospinning process, a strong electric field is applied between the syringe needle and the grounded metallic collector using a high voltage supply [27]. When the electrostatic force overcomes the surface tension of the polymer solution, a charged jet is driven out from the droplet created at the capillary tip. The charged jet is constantly stretched by the electrical force, and experiences bending instabilities while moving towards the collector. When the solution jet moves from the tip of capillary to the collector, the solvent evaporates and the jet becomes thinner more and more. Finally, solidified nanofibers are deposited on the metal collector in the form of a nonwoven web [28-31].

N. Sabetzadeh is with the Department of Textile Engineering, and the Group of Nanotechnology Engineering, Amirkabir University of Technology, Tehran, Iran. A. Gharehaghaji is with the Group of Nanotechnology Engineering, Amirkabir University of Technology, Tehran, Iran. Correspondence should be addressed to A. Gharehaghaji (E-mail: *aghaji@aut.ac.ir*).
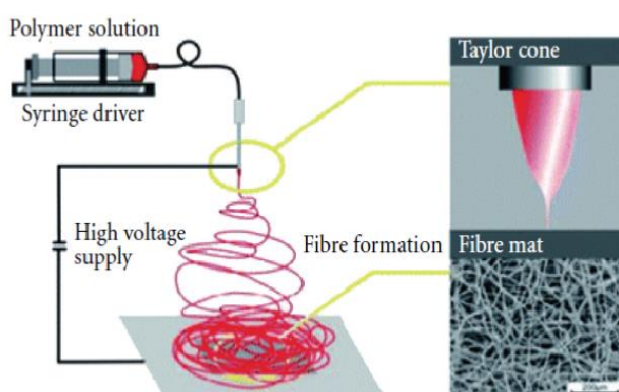
Fig. 1. A schematic drawing of a typical electrospinning setup [32].

The most effective parameters influencing morphology and diameter of electrospun nanofibers have been classified in four categories: polymer properties, polymer solution properties, processing conditions and ambient parameters. According to literature, applied voltage, solution flow rate, solution concentration, molecular weight of the polymer and nozzle to collector distance have a dominant effect on the morphology of nanofibers electrospun from many polymers such as polyethylene oxide (PEO), polyacrylic acid (PAA), polyvinyl alcohol (PVA), polyurethane (PU), polyacrylonitrile (PAN) and polycaprolactone (PCL) [33-36].

Considering the end-use applications, controlling of electrospinning conditions and parameters is of primary importance. Some exceptional structures such as core/shell, multichannel tubular structure, hollow, and porous nanofibers can be achieved by imposing changes on conditions and parameters of electrospinning process. Recently, there has been a great attention on developing of these high capability constructions for many application fields such as filtration, sensors, tissue engineering, drug delivery, superconductors, energy storage and super absorbers [7,37,38].

B. Porosity

The porosity is defined as the percentage of the pores volume to the total volume. Porous materials are defined as solids having a porosity of 20%-95% [37,39]. These materials can be categorized according to their pore size, pore shape, material type, and production method. Classification by pore size and by pore shape is more useful in applications of porous materials. According to the IUPAC recommendations, porous materials are classified as microporous (pore dimensions <2 nm), mesoporous (2-50 nm), and macroporous (>50 nm) [40,41]. Controlling the size and distribution of porosity could generate particular properties for porous materials that is required in a definite area of applications. In another point of view, porous materials are classified into two types: those containing open pores and those containing closed pores. It is a crucial notion that properties of porous materials could be varied depending on the nature of the materials, pore geometry, porosity, and pore size [39,42].

The term nanoporous material is implicit to comprise all kinds of porous solids that possess pore sizes within the range of 0.2 up to 50 nm [43]. In recent years, nanoporous materials have been recognized as promising candidates for the multifunctional applications such as catalysis, ion-exchange, energy storage, sensors, drug delivery, fuel cell membranes, tissue engineering and supercapacitors [7,41,42,44-47] due to their high specific surface area, more active sites, abundant inner space, and heterogeneous interfaces, which are essential to the physicochemical properties of materials [48]. Since the interior structure plays an important role in determining the material properties, various nanoporous materials with complex inner structures have been fabricated, such as hollow structures, multilevel structures, and many other special morphologies and shapes. In particular, nanoporous fibrous materials have fulfilled many needs in these areas because they can offer an intrinsically high surface area, inter-fiber pores and engineering versatility [46,48].

C. Porous Nanofibers

Recently, developed porous materials are in a great appeal for a wide range of applications due to their high surface area to volume ratios and larger pore volumes. Among these materials, porous nanofibers are being paid more and more attention in recent few years. Coupling ultra-fine diameter of nanofibers with their nanoporous structure could lead to the highest possible specific surface area, plentiful pores and excessive adsorption capacity resulting in further improvement in many appeals such as filtration, tissue engineering, catalysts, energy storage, sensors, adsorption, supercapacitors and conductors [6,7,46,49-51]. A brief overview on the current available techniques for fabrication and characterization of porous nanofibers and their applications is presented here.

D. Fabrication Mechanisms

In general, for producing porous nanofibers four fabrication mechanisms can be envisaged: (i) selective dissolution technique, (ii) selective pyrolyzate composite formation, (iii) phase separation and (iv) breath figure during electrospinning process [6,7,27,37,52,53]. In selective dissolution and selective pyrolyzate procedures, the porous structure is generated through electrospinning followed by an after treatment process. Phase separation and breath figure mechanisms create porous nanofibers when the fluid jets move from needle to collector during electrospinning process. More details of the fabrication mechanisms of porous nanofibers are followed.

1) Selective dissolution technique

Commonly, there are several ways for fabricating porous nanofibers by selective dissolution method. In one approach, porous structure can be prepared via electrospinning of polymer blend solutions followed by selective removal of one component. Another methodology is the inclusion of additives such as nanoparticles or salts in the solution followed by their removal in post electrospinning processes. Using of nanofibers as a template and then eliminate the template is another method. Here, some recent works that used these attitudes are reviewed throughout three divisions: (i) remove of

nanoparticles and additives, (ii) remove of nanofibers template, and (iii) remove of one polymer component.

Removing of nanoparticles and additives

Several research works have adapted this method. PAN/NaHCO$_3$ composite nanofibers were electrospun, and then NaHCO$_3$ was removed by a selective dissolution and reaction with a solution of hydrochloric acid. The obtained nanofibers showed highly porous surface after extraction of NaHCO$_3$ [50]. In similar work, porous PAN nanofibers were produced by selective removal of the silica nanoparticle component from PAN/silica composite nanofibers using hydrofluoric (HF) acid [54]. Khan *et al.* [55] showed removal of salt from the electrospun fibers of nylon-6/GaCl$_3$ complex using water which resulted in the generation of nanosized pores in nylon 6 nanofibers. Carbon nanofibers (CNFs) were prepared from PAN-incorporated with iron oxide nonparticles using electrospinning method [56]. In another research, creation of nanofibrous PAN/calcium carbonate (CaCO$_3$) nanocomposite was done through electrospinning process. The CaCO$_3$ nanoparticles were leached from the fibers in hydrochloric acid bath for producing an ultimate nanoporous structure. Morphological observation showed nanofibers with a diameter in the range of 270–720 nm containing nanopores of 50–130 nm [57].

Removing of nanofibers template

A mesoporous silica nanofibrous template was used for fabricating mesoporous carbon nanofibers (MC) [58]. The MC nanofibers were formed by filling the template with a carbon source followed by polymerization and carbonization processes, and removal of the silica template [58]. Fabrication and characterization of silver nanofibers with very high porosity using electrospun poly (vinyl chloride) (PVC) nanofibers as a template has also been reported [59]. Silver metal was deposited on PVC nanofibers by thermal evaporation. After the coating was complete, PVC and silver was immersed in tetrahydrofuran (THF) to remove the PVC molecules [59]. Yen Wei *et al.* [60] employed a viscous solution (of prehydrolyzed tetramethyl orthosilicate, β-D-glucose and PVA) as electrospinning solution to produce nanoporous silica nanofibers. The nanofibers were washed with phosphate buffer solution to extract out the glucose template and PVA. Porous SnO$_2$ nanofibers were arranged through electrospinning of PVA/SnCl$_4$·5H$_2$O composite and oxygen plasma etching. It was found that highly porous SnO$_2$ nanofibers had an average diameter of ∼20 nm; and the diameter of SnO$_2$ particles was ∼7 nm [61].

Removing of one polymer component

Composite nanofibers of gelatin (Gt)/PCL were devised by immiscible biopolymers of Gt and PCL. Porous nanofibers were created by removing the gelatin molecules in a solution of phosphate buffered saline [44]. Tran and Kalra [62] fabricated porous Nafion nanofibers through electrospinning of a mixture of Nafion and PAN trailed by confiscating of PAN nanofibers. For removing PAN from Nafion/PAN nanofibers and generation of pores, the electrospun nanofibers were flooded first in boiling water and then in sodium thiocyanate (NaSCN) solution. In another study, porous PAN nanofibers were produced by electrospinning of PAN and polystyrene (PS) blends, followed by selective dissolution of the PS portion in chloroform [46]. Production of porous ultra-fine poly(vinyl cinnamate) (PVCi) fibers via photo-crosslinking was reported by Youk *et al.* [63]. PVCi/poly(3-hydroxybutyrate-co-3-hydroxyvalerate) (PHBV) blend fibers were electrospun and then the PVCi was photo-crosslinked by UV irradiation. After the photocrosslinking of PVCi, PHBV was extracted from the blend fibers by using chloroform. PAN nanofibers with controllable nanoporous structures were prepared via electrospinning of PAN and polyvinylpyrrolidone (PVP) [51]. To remove PVP, the bicomponent nanofibers were extracted with water. By altering the ratio of PAN/PVP, the pore size and pore distribution of porous PAN nanofibers were controlled easily [51]. Wendorff *et al.* [64] used selective removal of individual polymer compounds to investigate porous structure of polylactide (PLA) and PVP nanofibers. A meaningfully different result was gained if either PLA or PVP was the main constituent. Ultrafine PGA/PLA blend fibers were electrospun and then PLA was removed via a selective dissolution technique with chloroform to prepare porous ultrafine (PGA) fibers [65]. Porous PAN/polyvinyledenfluoride (PVdF) nanofibers were produced by electrospinning of PAN/PVdF/PMMA blend and then the PMMA was separated by chloroform. After removing of the PMMA, the PAN/PVdF nanofibers had highly porous surface [66].

2) Selective pyrolyzate composite formation

In this method, thermal treatments such as carbonization, calcination and oxidation are used after production of nanofibers to generate porous structure. Some porous nanofibers were produced by selective pyrolyzate method but according to the production process of carbon nanofibers, most reports in this section were regarded to porous carbon nanofibers fabrication.

CNFs containing Ni nanoparticles were synthesized by carbonization of electrospun PAN nanofibers including NiCl$_2$ followed by low-temperature activation in oxygen atmosphere [67]. Addition of Ni nanoparticles produces a porous structure due to their catalytic role, which can increase the specific adsorption capacity of the activated CNFs [67]. In another study, porous LaFeO$_3$ nanofibers were invented by calcination of PVP/[La(NO$_3$)$_3$+Fe(NO$_3$)$_3$] composite electrospun nanofibers [68]. Li *et al.* prepared a phenolic resin-based mesoporous CNFs through electrospinning shadowed by carbonization and removal of SiO$_2$. The mesoporous nanofibers exhibited high surface area, large pore volume, and narrow pore size distribution [48]. In another work, porous SnO$_2$ nanofibers were fabricated by electrospinning of PVP and SnCl$_4$.5H$_2$O pursued by oxygen plasma and annealing treatment [69]. In a different approach, porous hollow SnO$_2$ nanofibers were successfully prepared by electrospinning of PVP/Sn precursors/dual solvents system and calcination treatment [70]. A recent study shows macroporous silica hard-

template which was used to synthesize mesoporous carbon nanofibers. Removing silica from the carbon walls during carbonization process resulted in porosity [71]. Yu et al. [45] produced porous nickel oxide (NiO) and zinc oxide (ZnO) submicron- and nanofibers by infusing electrospun PAN fiber templates with corresponding metal nitrate aqueous solutions and subsequent calcination. The PAN fiber templates were removed through decomposition, carbonization, and oxidation due to reaction with O_2 in air. In a recent research, porous CNFs were prepared by stabilization and carbonization of PAN nanofibers containing $Si@SiO_x$ nanoparticles [72]. Porous $LiNb_3O_8$ nanofibers were successfully prepared through electrospinning and an annealing process. The obtained porous $LiNb_3O_8$ nanofibers were composed of interconnected nanocrystals and many nanopores [73].

Porous hollow CuO and Cu nanofibers were achieved through electrospinning of a PVP/copper acetate $(Cu(CH_3COO)_2)$ solution followed by annealing and reduction [74]. In a research study, calcinations of $TiO_2/ZnCl_2/PVP$ nanofibers resulted in porous TiO_2/ZnO composite nanofibers [75]. Macroporous silica nanofibers were fabricated by calcination of electrospun silica nanoparticles and polymeric microspheres [76]. In a similar research, nanoporous silica nanofibers with ultra-high specific surface area were developed using the solutions of PVA and colloidal silica nanoparticles by electrospinning, followed by selective removal of the PVA component by calcination [47]. $LaFeO_3$ ribbon-like porous nanofibers were created by electrospinning utilizing sol–gel precursors and heat treatment at 600 °C [77]. Core-shell porous CNFs with Pt catalysts were explored by co-electrospinning and a reduction method [78]. A mixture of PAN and a copolymer of acrylonitrile and methyl methacrylate (poly(AN-co-MMA)) in DMF was electrospun into submicrometer fibers with a microphase-separated structure. Oxidation process was followed and the copolymer domains were pyrolyzed consequently, resulting in an ultrathin nanoporous CNFs that was preserved after carbonization [40]. In another study, a blend of PAN and poly-Llactic acid (PLLA) in DMF was applied to prepare porous CNFs via electrospinning and subsequent thermal treatments [79]. Ji and Zhang [80] organized carbon/Si composite nanofibers with porous structures by stabilization (in air) and carbonization (in argon) of electrospun PAN/PLLA/Si composite nanofibers. Porous inorganic nanofibers were fabricated by a microemulsion (metal alkoxide precursor, oil, surfactant, and solvent) electrospinning approach. After removing organics by calcination, hierarchically structured ultraporous TiO_2 nanofibers were obtained. The procedure for the fabrication of porous nanofibers is illustrated in Fig. 2 [48].

Selective thermal degradation of electrospun poly etherimide/poly (3-hydroxybyrateco-3-hydroxyvalerate) (PEI)/(PHBV) fibers led to porous ultra-fine fibers. PEI and PHBV were partially miscible and phase separation proceeded rapidly during the electrospinning process [37]. Electrospinning of a PAN/PLLA blend solution was

followed by carbonization at different temperatures and in various atmospheres for generation of porous CNFs, in a research reported by Ji et al. [81]. Yang et al. [82] fabricated PAN/PMMA fibers containing graphene by electrospinning method and hierarchical porous CNFs were obtained after subsequent heat treatment. Activated carbon nanofibers with hollow core/highly mesoporous shell structure were obtained by concentric electrospinning, and subsequent processes of stabilization, carbonization, and activation. Fabrication process is shown in Fig. 3 [83].
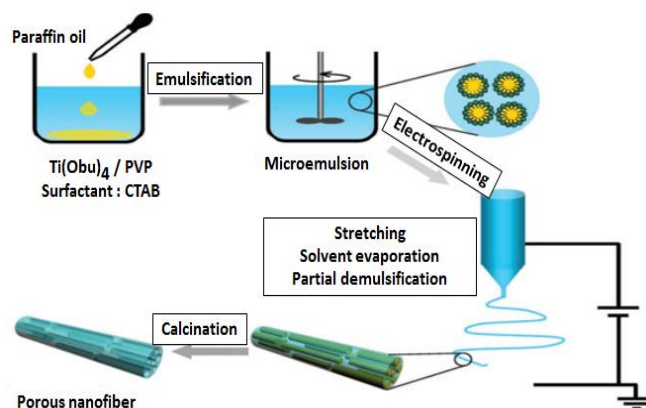

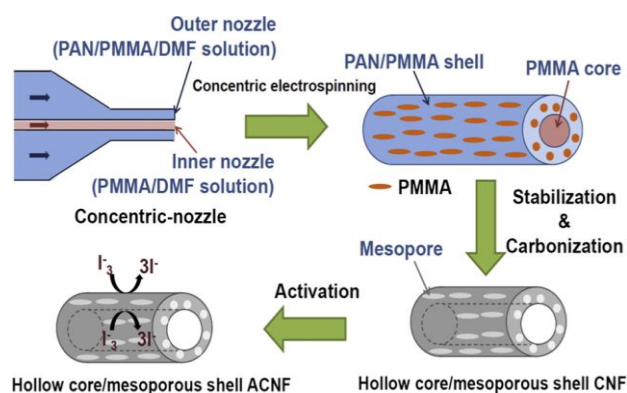Fig. 2. Fabrication procedure of porous oxide nanofibers [48].

Fig. 3. The fabricating process and I^3 reduction of activated carbon nanofiber with hollow core/mesoporous shell structure (Meso-HACNF) [83].

Synthesis of carbon-coated Li_3N porous nanofibers via electrospinning was reported by Xia et al. [84]. In another research, porous CNFs in the form of thin webs with the help of zinc chloride were produced by Kim et al. [85]. During a thermal treatment, suitable pores were created on the outer surface of CNFs [85]. A similar structure involving Mn oxide-loaded porous CNFs were formed by electrospinning of PAN solutions containing different amounts of $Mn(CH_3COO)_2$, followed by thermal treatments in different environments [50]. Hierarchical porous, magnetic $Fe_3O_4@carbon$ nanofibers were achieved by using electrospun PAN/polybenzoxazine (PBZ) nanofibers as a composite carbon precursor [86]. By combining the precursor design and the activation process, a series of $Fe_3O_4@CNFs$ with tunable porous structure

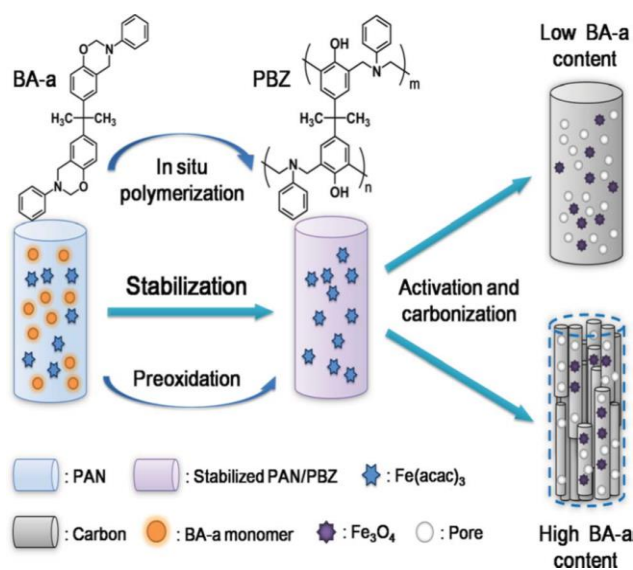were obtained. Synthesis procedures are shown in Fig. 4 [86].

Fig. 4. Synthesis procedures of A-FeCNF and the relevant formation mechanisms [86].

Nanoscale porous CNFs were produced by self-degradation template method with an average pore diameter of 27.98 nm [87]. Potassium hydroxide (KOH) and zinc chloride (ZnCl$_2$) activations were used to increase specific surface area and pore volume of CNFs. It is believed that KOH activation is much more effective in increasing the specific surface area and the total pore volume than ZnCl$_2$ activation [88]. Jin *et al*. [89] fabricated highly porous CNFs by chemical activation of electrospun PAN nanofibers. Interestingly, with a rise in the activation temperature, the pore structure changed from a micropore structure to a mesopore structure.

3) Breath figure and phase separation mechanisms

Breath figures occur due to evaporative cooling as a result of rapid solvent evaporation while the electrospinning jet travels from the syringe to the collector. As the surface of the jet cools, moisture from the air condenses on the surface of the fibers and grows in the form of dews. The dews remain as individual units acting as hard spheres owing to convection currents on the surface of the jet. As the fiber dries, the water dews leave an imprint on the surface of the fibers in the form of pores [23,27,90,91]. Phase separation is another mechanism for the formation of pores on the surface of electrospun nanofibers. Decreasing temperature, loss of solvent, or increase in nonsolvent (moisture) causes a solution to become thermodynamically unstable during the electrospinning process, which drives phase separation and results in porosity [92]. Actually, rapid solvent evaporation causes phase separation into polymer-rich and solvent-rich areas. The evaporation of the volatile solvent leaves behind voids thus porosity in the nanofiber is attained [93,94]. There are various phase separation methods to prepare porous membranes such as thermally induced phase separation (TIPS), vapor-induced phase separation (VIPS),

immersion precipitation and air-casting of the polymer solution [24,27,92,95]. The most pertinent phase separation procedures for porous nanofiber formation are TIPS and VIPS. In TIPS, phase separation occurs by lowering the temperature of the solution as the fiber passes through the distance between the needle and the collector [95,96]. The VIPS method involves the penetration of a nonsolvent vapor causing phase separation in the polymer solution. The miscibility of nonsolvent (water) with solvent causes creation of liquid-liquid phase separation and finally porous features within the fibers occur 24,94,95,97].

It is clear that the creation of porosity during electrospinning is more complex than other procedures since the nanofibers are carrying charge, which is not present in other pocedures. On the other hand, the increase in the jet surface area occurs within milliseconds which can lead to a number of thermodynamically driven events [95]. Accordingly, porous structure is the outcome of numerous mechanisms such as breath figure, TIPS, and VIPS through the travel of the jet from the syringe to the collector. So far, various studies have shown the occurrence of these mechanisms in the porous nanofiber creation, which are mentioned in the following section.

Highly porous PMMA hollow nanofibers were obtained by coaxial electrospinning of outer polymer solutions and inner silicon oil with a highly volatile solvent. Pore formation occurred at the outer surface of the hollow fibers due to rapid solvent evaporation [98]. Partially crystalline PLLA and two amorphous polymers, polycarbonate (PC) and polyvinylcarbazole, were used for formation of porous nanofibers. The structure development was controlled by a rapid phase separation induced by the evaporation of the solvent and a subsequent rapid solidification [99]. Electrospun polymer nonwoven mats with porous surface morphology were fabricated by varying the collector temperature during electrospinning [27]. It was observed that the surface morphology, porous structure, and the properties such as pore size, depth, shape, and distribution of the nonwoven mats were greatly influenced by the collector temperature [27]. By immersing the collector in a bath of liquid nitrogen, porous PAN nanofibers were achieved through TIPS between the solvent-rich and solvent-poor regions in the fiber during electrospinning, followed by the removal of solvent [100].

Porous PS fibers were electrospun from various DMF solutions at different weight fractions under relative humidity of 35%. The development of porosity is attributed to the liquid-liquid phase separation of water molecules in atmospheric moisture and DMF [93]. Xu *et al*. produced PAN porous nanofibers in one step by electrospinning of a ternary system of PAN/DMF/water at ambient environment. The development of porous structure was mainly due to the spinodal decomposition phase separation which happened during the electrospinning process. At the critical water concentration, where a homogeneous ternary solution could be maintained, porous fibers were generated [101]. Interior porosity was observed in PS fibers electrospun from solutions of PS in DMF, and

a humid environment. The formation of interior porosity was attributed to the miscibility of water (as a nonsolvent) with DMF [96]. Using a nonsolvent bath as a collector for electrospun submicrometer fibers is an efficient method to persuade porosity. The presence of remaining solvent in the nanofibers causes phase separation when the fibers reach the nonsolvent bath [102]. The effects of polymer solution concentration, composition of the solvents mixture, and applied voltage on polyvinylbutyral (PVB) nanofibers porosity and diameter were investigated in the work reported by Lubasova [52]. It was found that the PVB fibers obtained from the solvent mixture THF /dimethylsulfoxide (DMSO) (9/1 v/v) exhibit a highly porous structure with a pore size of approximately 100 nm [52]. In a recent study, surface of PLLA electrospun fibers became porous after evaporation of highly volatile solvent in controlled humidity and temperature. Changes in the concentration of PLLA solution resulted in the fibers with different surface porosity [103]. Ding *et al.* fabricated PS fibers with micro/nanoporous structure in the core and/or on the fiber surfaces during electrospinning by varying solvent composition and concentration of the PS solutions. The THF/DMF mixing ratio in PS solutions affected porous structure by phase separation resulting from rapid evaporation of the solvent [94]. The influence of solution concentration, spinning voltage, flow rate of the solution, and the needle to target distance on porous morphology of crystalline and amorphous polymeric nanofibers, including PC, PEO, and PMMA were investigated in another research [95]. Also, effect of humidity and molecular weight in the porosity of PS nanofibers were studied. VIPS and TIPS were the most relevant phase separation processes which explained the pore formation in the PS electrospun fibers [24]. PLA with different crystallization ability were electrospun from a mixed solvent of DCM and DMF into porous nanofibers through two types of spinnerets: e nozzle and channel spinnerets, in a highly humid environment. Results showed that the surface morphology of porous nanofibers was influenced by take-up velocity and crystallization ability of the polymer. This influence was clearer in the case of channel-based spinneret and PLA with low crystallization ability. A schematic drawing of the two types of spinnerets is shown in Fig. 5 [104].
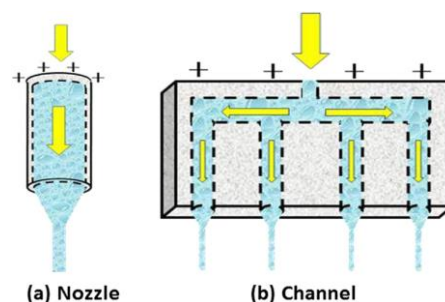

Fig. 5. A schematic drawing of two types of spinnerets: (a) nozzle, and (b) channel [104].

Ultrafine porous cellulose triacetate (CTA) fibers were prepared by electrospinning with MC and a mixed solvent of MC/ethanol (EtOH) and their pore structures was investigated [105]. Ultrafine porous fibers electrospun from MC had isolated circular shape pores with narrow size distribution. These porous structures were induced by phase separation resulting from the rapid evaporation of solvent during the electrospinning process [105]. Highly porous PLLA fibers were produced by electrospinning a ternary system of nonsolvent (butanol)/solvent (dichloromethane)/poly(L-lactic acid) [106]. During the electrospinning, the evaporation of solvent and nonsolvent causes the composition of polymer fluid jet to enter the two phase region of the ternary phase diagram, since the solvent is more volatile than the nonsolvent. Thus the jet yielded to different phase separated structures, and further evaporation of the residual nonsolvent could lead to porous fibers (Fig. 6) [106].

By immersing the collector into a bath of liquid nitrogen, porous polymer fibers were obtained through TIPS between the solvent-rich and solvent-poor areas [107]. In this method, the fibers hit a bath of liquid nitrogen before reaching the collector. The remaining solvent is frozen along with the polymer. In the freezing process, phase separation into solvent-rich and solvent-poor regions is induced [107].

D. Characterization

SEM is mainly used for imaging the surface of materials [2] and it is applied mostly for investigation of nanofibers surface morphology. Surface porosity of several polymeric and mineral nanofibers has been studied by SEM.
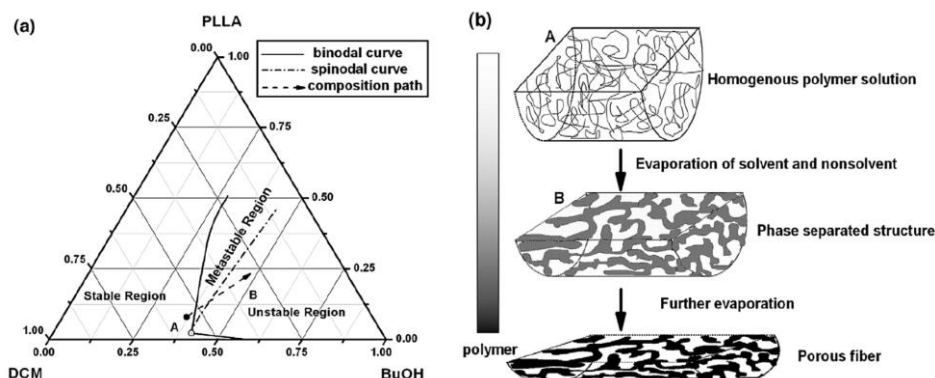

Fig. 6. (a) Calculated phase diagram of butanol/dichloromethane/PLLA system. (b) A schematic representation of the process of porous fiber formation during electrospinning [106].

Fig. 7 shows SEM micrographs of highly porous PC hollow nanofibers fabricated by coaxial electrospinning with a highly volatile solvent. The interior surface was quite smooth. Hence, pore formation happened at the outer surface of the nanofibers due to rapid solvent evaporation [98].
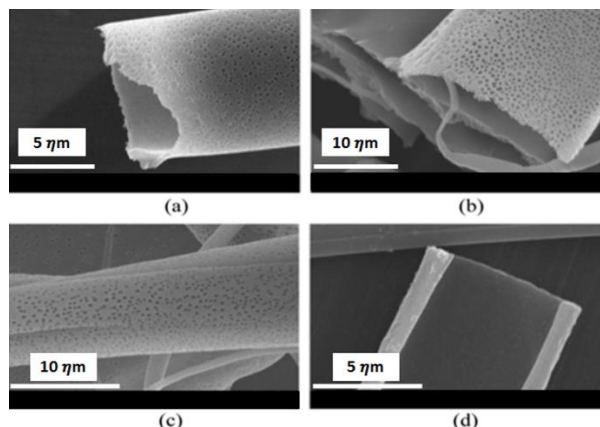

Fig. 7. SEM micrographs of porous hollow nanofibers with different molecular weight (Mv) of PC. (a) 17,000, (b) 22,000, (c) 30,000 and (d) 30,000 g mol^{-1} [98].

Effect of collector temperature on the porous structure of electrospun PLLA nanofibers is presented in SEM micrographs of Fig. 8. Differences in the nanofibers structure due to the increasing in temperature could be observed obviously [27].
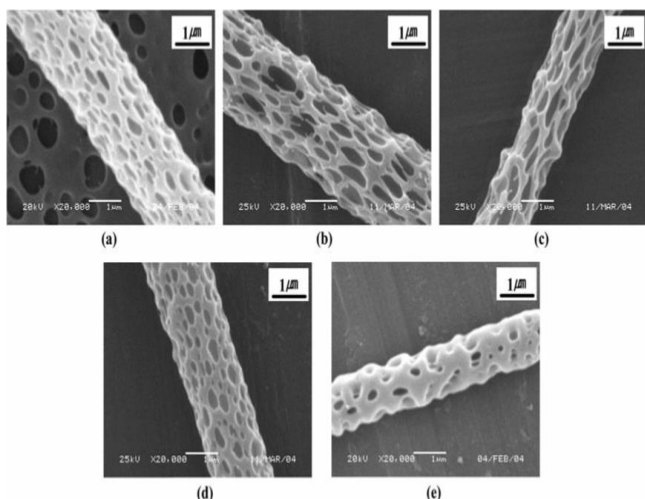
Fig. 8. SEM images of electrospun PLLA nanofibers as a function of collector temperature; (a) room temperature (21 ^{o}C), (b) 40, (c) 50, (d) 60 and (e) 70 ^{o}C [27].

Molecular weight effect on the atactic poly(methyl methacrylate) (aPMMA) nanofibers structure could be seen in SEM images of Fig. 9. The electron micrographs in Fig. 9 demonstrate that fibers from two different molecular weights (M_w ~ 350000 and 996000) of aPMMA were porous. In spite of the molecular weight difference of the two aPMMA samples, the bead-free porous fibers developed at the same concentration with comparable pore size and shape [92].
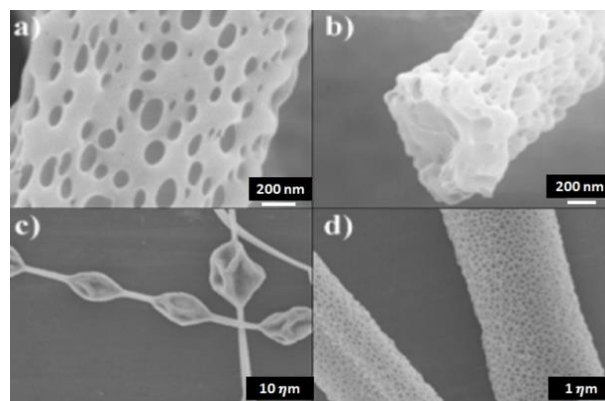

Fig. 9. Porous fibers from aPMMA/MC from Mw of 350000 g mol^{-1} (a) 10 wt % and (b) 12 wt % and from Mw of 996000 g mol^{-1} (c) 10 wt % and (d) 12 wt % [92].

There are some other research works that have used SEM for the investigation of porosity in the structure of other nanofibers such as PCL [44], PVB [52], CNFs [78,108], SnO$_2$ [70], Silver [59], TiO$_2$ [48], LaFeO$_3$ [77], PLLA, PC and polyvinylcarbazole (PVK) [99], and PS nanofibers [24].

TEM images provide topographical, morphological, compositional and crystalline information of samples on a molecular level. Usually, it is used for the investigation of nanofiber inner structure. TEM has been used for analysis of nanofiber porosity in many research works extensively.

The morphology and microstructure of porous LiNb$_3$O$_8$ nanofibers were presented in detail by TEM. Fig. 10(a) indicates that the LiNb$_3$O$_8$ nanofibers possess porous morphology with a diameter of 200 nm. At a higher magnification (Fig. 10(b)), many mesopores can be clearly observed within the whole fiber [73].
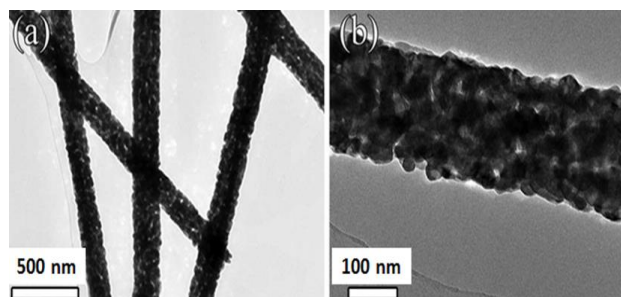

Fig. 10. TEM images of LiNb$_3$O$_8$ nanofibers [73].

Porous structure of TiO$_2$ and ZnO nanofibers was investigated using TEM images that are presented in Fig. 11. The TiO$_2$ and ZnO nanofibers (Fig. 11(d) and 11(e)) are smoother than TiO$_2$/ZnO nanofibers and the average diameter of TiO$_2$/ZnO nanoparticles was about 40 nm (Fig. 11(f)) [75].

In another research, TEM was applied to study porous structure of CNFs made from PAN/PLLA (9:1) nanofibers. According to Fig. 12, the irregular surface morphology with elongated indents and clear ridges along the fiber surface indicate the presence of large pores (i.e., meso-pores with diameters in the range of 2–50 nm) [79].
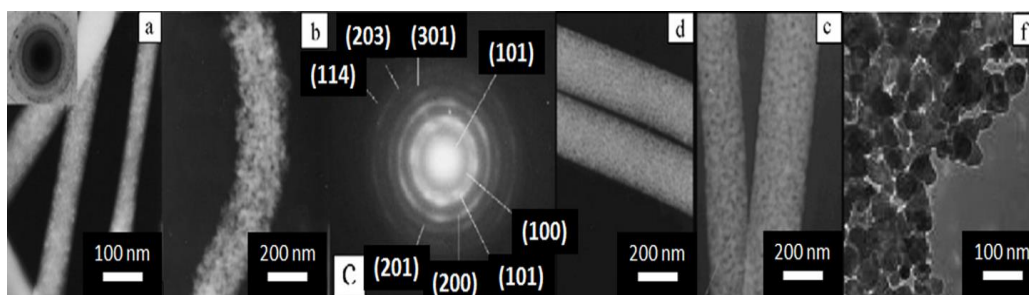
Fig. 11. TEM and ED pattern of (a) TiO2/ZnO nanofibers before calcinations, (b and c) after calcinations, (d) TiO2 nanofibers, (e) ZnO nanofibers and (f) TiO2/ZnO nanoparticles [75].
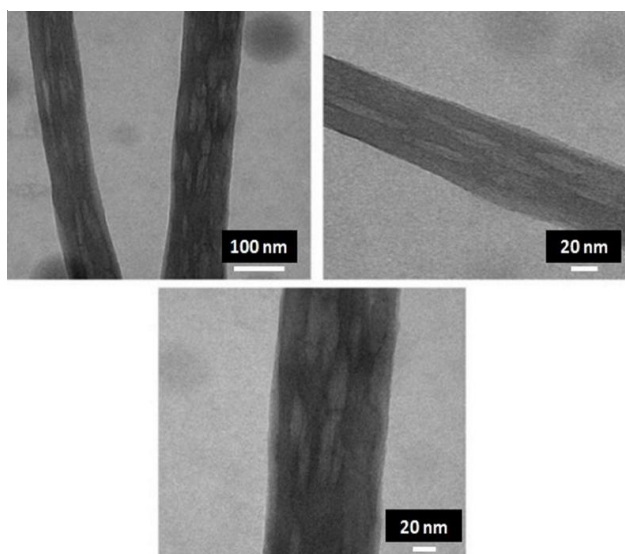

Fig. 12. TEM images of porous CNFs made from PAN/PLLA (9:1) nanofibers [79].

Applying TEM for the analysis of nanofiber porosity also has been reported for CNFs [50,56,71,108], SnO_2 [70], Nafion and PAN [46,62], TiO_2 [48], CuO [74], $LaFeO_3$ [77], Nylon-6 [55], PS nanofibers [96] and etc.

The AFM relies on a scanning technique to produce very high resolution, 3-D images of sample surfaces [109] in comparison with both SEM and TEM techniques that essentially yield two-dimensional representation of nanofibers and pores [5]. Hence, AFM was used mostly for measuring the depth and diameter of nanofiber pores. Moreover, using of AFM for determining the porosity percentage was reported.

To determine the porosity of PVDF nanofibers, a microsized piece of nanofibers was cut using the tip of AFM and was glued to it. The fiber weight was determined by the change in the tip resonance frequency. Then, the fiber was immersed into Galwick (Porous Materials, Inc). Becuase Galwick has very low surface tension, it wets PVDF surface and fills the fiber pores. New value of the resonance frequency of the wet fiber-cantilever system was used to calculate the weight of wet fiber. Finally, fibers porosity was estimated using the volume of Galwick that penetrated into pores [110]. In another study, AFM images were recorded to study the effect of the collector temperature on the pore properties like pore depth, pore diameter, and surface area of electrospun PLLA [27]. The details of pore depth and surface area of the electrospun

PLLA fibers at different collector temperatures are presented in Table I. Similar investigations were conducted in this work for PS nanofibers [27].

TABLE I
PORE DEPTH AND SURFACE AREA OF ELECTROSPUN PLLA NONWOVEN
MATS AS A FUNCTION OF COLLECTOR TEMPERATURE [27]

collector temperature (°C)	range of pore depth (nm)	average of pore Depth (nm)	surface Area (μm^2)[a]
RT	80-180	160	13.67
40	90-290	210	15.9
50	110-460	270	16.12
60	100-270	180	14.4
70	30-150	110	11.33

[a]The projected surface for all the $3\times3\mu m^2$ images presented in this table is $9\mu m^2$.

The AFM was used for considering the PS nanofibers pore structure in a similar research work. AFM measurements reveal that the depth of the pores increases as the relative humidity and molecular weight increase. AFM analysis allowed the calculation of surface area of the porous PS fibers. The projected surface area for all the 3×3 μm images presented in Fig. 13 is 9 μm^2. The calculated surface area for the images in Fig. 13 (a-d) is 12.4, 14.9, 10.67, and 12.1 μm^2, which is equal to a 30-65% increase in the surface area of the fiber [24].

Various general techniques are available for characterization of porous materials such as Mercury Intrusion Porosimetry, Liquid Extrusion Porosimetry, Capillary Flow Porometry and Brunauer, Emmett, and Teller (BET). BET is the most widely used method for estimating nanofibers surface area and porosity. Actually, some of these techniques are more appropriate for stiffer materials and may not be applied to nanofibers of all organic polymers. On the other hand, some methods can not characterize pores smaller than macropores [5,38,111]. BET analysis provides specific surface area evaluation of materials by nitrogen multilayer adsorption measured as a function of relative pressure using a fully automated analyzer. The technique involves exterior area and pore area approximations to determine the total specific surface area in m^2 g^{-1} incoming significant information in studying macroporous, mesoporous and microporous materials. The main idea of the theory is an extension of the Langmuir theory, which is concerned with monolayer and multilayer molecular adsorption [5]. Using of BET method in many

studies on nanofiber porosity represented useful information such as specific surface area, total pore volume, average pore size and average pore width.
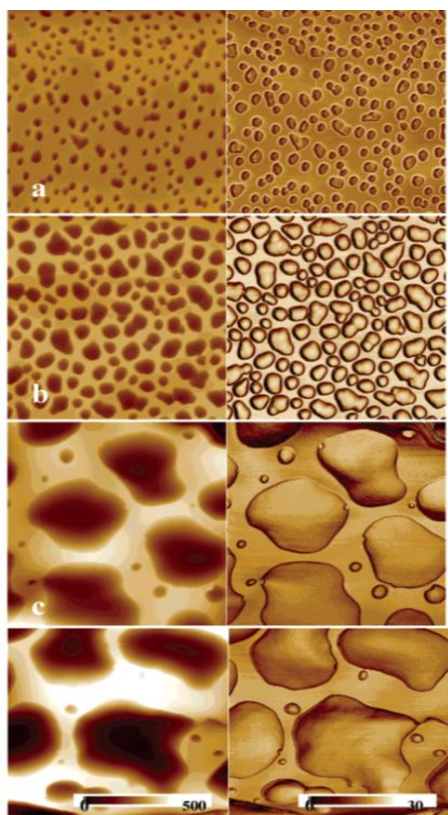

Fig. 13. AFM images, topography (left), phase (right) (a) 190000 g mol^{-1} PS fibers under 50-59% humidity, (b) 190000 g mol^{-1} PS fibers under 60-72% humidity, (c) 560900 g mol^{-1} PS fibers under 50-59% humidity, (d) 560900 g mol^{-1} PS fibers under 60-72% humidity [24].

The BET method was utilized to estimate the specific surface areas of mesoporous CNFs. By using the Barrett–Joyner–Halenda (BJH) model, the pore volumes and mesopore size distributions were derived from the desorption branches of isotherms. The micropore volumes and micropore surface areas were measured from the V-t plot method. Horvath Kawazoe (HK) method was used to obtain the micropore size distribution. The calculated pore size distribution of three samples (C-1, C-2, and C-3) with different pore 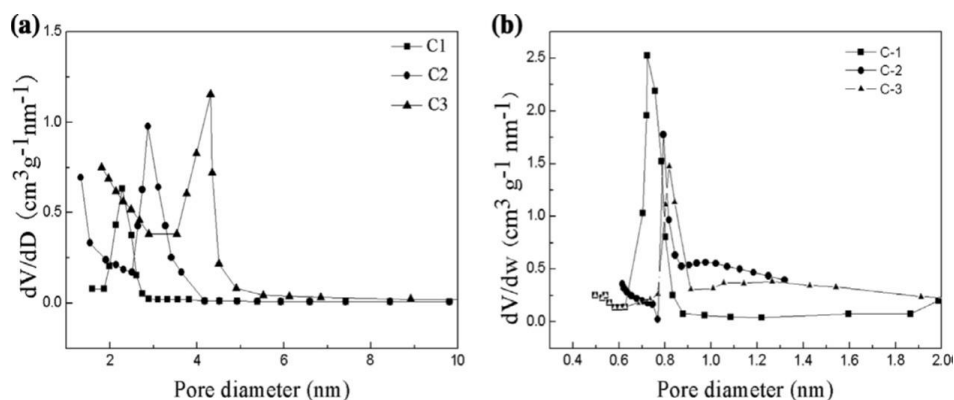textures are shown in Fig. 14, respectively. It illustrates that CNFs have typical type-IV isotherm with a N_2 hysteresis loop in all samples, suggesting mesopores in CNFs [49].

BET measurements were done to assess the surface area of the porous hollow SnO_2 nanofibers. The N_2 adsorption–desorption isotherm curve of the porous SnO_2 fibers exhibited the characteristic of mesopore structures. The average pore size in the porous SnO_2 fibers was approximately 16.2 nm and the corresponding BET specific surface area was about 35.8 m^2 g^{-1} (BJH method) [70].

Table II summarizes the specific surface area and pore size observed at various molecular weights of hollow and porous PC nanofibers as determined by BET analysis. The specific surface area of fibers was very high and a slight decrease was observed with increasing PC molecular weight which was while the average pore size increased [98].

TABLE II
THE SPECIFIC SURFACE AREA AND AVERAGE PORE SIZE OF THE PC HOLLOW AND POROUS FIBERS [98]

molecular weight (Mv)/ viscosity (cP)	specific surface area (m^2 g^{-1})	average pore size (nm)
17000/430	3500	120±20
22000/1250	2900	130±30
30000/3150	2400	210±30

Surface area measurements of porous PAN nanofibers were carried out using BET nitrogen adsorption method. Porous nanofibers obtained by HF-treating PAN/silica (5 wt%) composite nanofibers had a surface area of 23.61 m^2 g^{-1}. In comparison, pure PAN nanofibers with similar diameters had a surface area of only 19.93 m^2 g^{-1} [54]. Kim *et al*. used BET to evaluate specific surface area and pore size distribution of the zinc-chloride-activated porous CNFs. With an increase in the added amount of zinc chloride, the amount of adsorbed N_2 was increased (Table III). This change demonstrated that the evolution of the porous structure on the surface of nanofibers was definitely caused by zinc chloride [85].

The pore structure of PAN/PBZ-based Fe_3O_4@CNFs was measured through N_2 adsorption to investigate the effect of precursor constitution and activation. As shown in

Fig. 14. Calculated (a) mesopore and (b) micropore size distributions [49].

TABLE III
SURFACE CHARACTERIZATION OF THE ZINC-CHLORIDE-ACTIVATED POROUS CARBON NANOFIBERS [85]

$ZnCl_2$ [wt%]	SSA [a] $[m^2 g^{-1}]$	TPV [b] $[cm^3 g^{-1}]$	V_{meso} [c] $[cm^3 g^{-1}]$	V_{micro} [d] $[cm^3 g^{-1}]$	W_{micro} [e] [nm]	W_{meso} [f] [nm]	APS [g] [nm]	Electrical conductivity [h] $[Scm^{-1}]$
1	310	0.17	0.03	0.15	0.15	5.3	0.54	1.418
3	420	0.22	0.03	0.20	0.20	6.5	0.54	1.400
5	550	0.34	0.10	0.26	0.26	6.9	0.59	1.390

[a] Specific surface area (SSA) was calculated by Brunauer–Emmett–Teller (BET) method. [b] TPV indicates total pore volume. [c] Vmeso is the mesopore (1.7–300 nm) volume calculated by Barret, Joyner, and Halenda (BJH) method based on Kelvin equation. [d] Vmicro is the micropore volume calculated by Horvath–Kawazoe (HK) method. [e] Wmicro is micropore volume calculated by HK method. [f] Wmeso is the average mesopore width calculated by BJH method. [g] APS indicates average pore width calculated by BET method (4V/A by BET). [h] The electrical conductivities were measured by four-point probe method.

Fig. 15 (a), all curves exhibited an isotherm of type II, and a series of typical adsorption behavior including micropore filling, monolayer adsorption, multilayer adsorption and capillary condensation could be observed. The moderate N_2 adsorption below $p/p_0 < 0.1$ and the continuous increase of N_2 adsorption over the region of $0.1 < p/p_0 < 0.9$ indicated the presence of both micropores and mesopores in CNFs. In addition, an obvious uptake occurring at $p/p_0 > 0.9$ exposed the existence of substantial slit shape pores. Interestingly, Fig. 15 (b) is showing the isotherms upon an extremely low pressure range ($p/p_0 < 0.01$) which reveals an unexpected micropore filling behavior [86].

Fig. 15. (a) N_2 adsorption isotherms of various FeCNF and A-FeCNF samples. (b) Nitrogen isotherms over a low pressure range (p/p$_0$ < 0.01) which show the microporous adsorption behavior of relevant samples [86].

Porous morphology of $LiNb_3O_8$ [74], hollow CuO and Cu [74], CNFs [50,56,79,88,89,112], TiO_2/ZnO [75] and PAN nanofibers [51] have been investigated using BET method.

E. Applications

The existence of porous structure in the electrospun nanofibers has led to a huge specific surface area that is an appropriate property for wide applications such as tissue engineering, drug delivery, adsorption/separation materials, catalysts, supercapacitors, energy storage, sensors, superhydrophobic materials, batteries, conductors, fuel cells, dye-sensitized solar cells and filtration. In recent years, fabrication of these convenient nanofibers due to their new and extended application zones has been endeavored greatly by a number of groups that are mentioned hereinafter.

1) Medical applications

There are various works conducted on application of porous nanofibers in tissue engineering. Some examples are reviewed here. Hepatocyte cell growth on PCL nanofibrous layers with different morphology was compared in a work reported by D. Lubasova [113]. On the porous PCL nanofibres, the hepacotyte attached well and exhibited a better growth than cells grown on non-porous PCL nanofibres [113]. Lee and co-workers developed a porous scaffold structure for a facile transport of metabolic nutrients and wastes through the nano sized pores and for the cell implantation and blood vessel invasion through the micro-sized pores [114].

Also, nanoporous silica nanofibers were employed as a matrix to encapsulate horseradish peroxide enzymes via electrospinning method. The nanofibers with mesoporosity displayed a greater activity than the conventional nontemplated silica samples and a greater activity than HRP immobilized silica powders [60].

2) Supercapacitors

Porous CNF mats were used as electrode materials for supercapacitors [108]. The produced porous CNFs exhibit high specific surface area with a large fraction of mesopores. Electrochemical measurements showed large specific gravimetric and volumetric capacitances due to the large portion of mesopores [108]. Thin layers consisting of porous CNFs for supercapacitors was produced by Chan Kim via the electrospinning of PAN solutions containing Zinc Chloride [85]. The higher surface areas of these fibrous materials showed higher specific capacitances. Porous CNF webs with 5 wt% zinc chloride revealed the
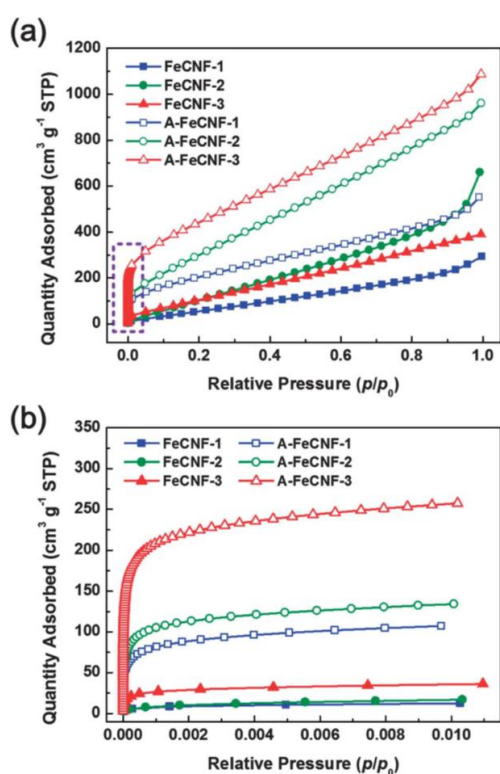
largest specific surface area, the highest capacitance and good rate capability because of their smaller nanofiber diameter and large specific surface area [85]. In other similar work, mesoporous CNF web was prepared by Kim and co-workers as electrode material for high-performance supercapacitors [82]. Hierarchically porous carbon nanofibers (HPCNFs) containing numerous electroactive heteroatoms showed excellent electrochemical performance (Fig. 16) and their thermal treatment with melamine results in nitrogen-doped HPCNFs (N-HPCNFs) with 9.1 at% nitrogen and improved electrical property.[89]
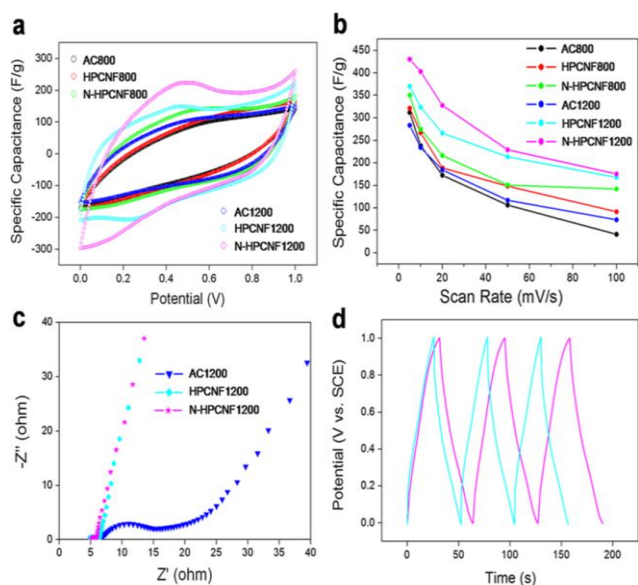

Fig. 16. (a) Cyclic voltammograms of all the samples at a scan rate of 5 mV s^{-1} over a potential range from 0 to 1 V in 1 M H$_2$SO$_4$ electrolyte, (b) specific capacitance of all the samples for different scan rates over a potential range from 0 to 1 V in 1 M H$_2$SO$_4$ electrolyte, (c) Nyquist plots of AC1200 (blue), HPCNF1200 (cyan) and N-HPCNF1200 (magenta) in the frequency range from 100 kHz to 0.1 Hz, and (d) galvanostatic charge/discharge curves of HPCNF1200 (cyan) and N-HPCNF1200 (magenta) over a potential range from 0 to 1 V in 1 M H$_2$SO$_4$ electrolyte. (For interpretation of the references to color in this figure legend, the reader is referred to the web version of this article.) [89].

Synthesis of MnO$_2$ nanoflakes/porous carbon nanofibers (PCNFs) for flexible supercapacitor electrodes with high performance was reported. The specific capacitance of the electrode is greatly improved with the increase in electrolyte temperature [115]. In another research work, supercapacitor electrodes consisting of porous NiO nanofibers were fabricated by electrospinning on Ni foam [116]. Activated carbon nanofibers (ACNFs) were prepared for supercapacitor electrode applications by using nanosize PAN fibers as a precursor, following treatments in different activation conditions. PAN-based CNFs were modified over a variation of activation time to prepare activated CNFs with high specific surface areas and mesopore structure [117]. A recent work reports a facile method to fabricate PCNFs via electrospinning of PAN/DMSO$_2$ pristine fibers followed by preoxidation and carbonization. The PCNFs showed an enhanced electrical double layer capacitance characteristic, confirmed by cyclic voltammetry [118].

3) Adsorption/Separation

Mesoporous CNFs were produced from phenolic resin and used in the adsorption of large dye molecules [49]. The relationship between the pore textures and adsorption properties was studied. It was suggested that the adsorption of different dyes depends on an appropriate pore size distribution in addition to surface area [49]. PAN/PBZ-based Fe$_3$O$_4$@CNFs with hierarchical porous structure demonstrated effectual adsorption of organic dyes in water and a fast magnetic separation property. The results indicated that the nanofibers showed an excellent adsorption ability in the removal of Methylene Blue (MB) and Rhodamine B (RhB) dyes [86]. Selective adsorption of oil from water was shown using porous PS nanofibers. It was found that the PS nanofibers formed at 45% RH have oil sorption capacities of 113.87 g g^{-1} and 96.89 g g^{-1} for motor oil and sunflower seed oil, respectively [119]. In another study, absorption test of MB dye in water by porous silica nanofiber membranes indicated large capacity for absorbing MB dye molecules due to their largest surface area. The color change of MB solutions is shown in Fig. 17 [47].
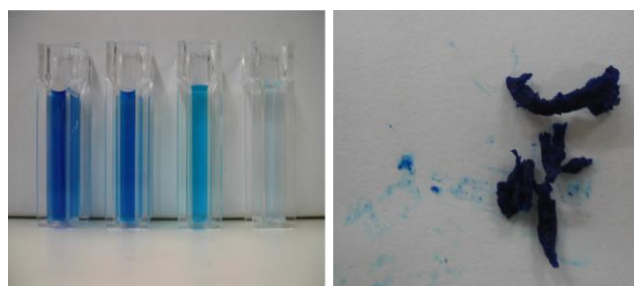

Fig. 17. Conventional digital camera images of (a) MB solutions after treatment with various fibrous samples and (b) the dried fibrous SiO$_2$ sample after immersion in MB solution [47].
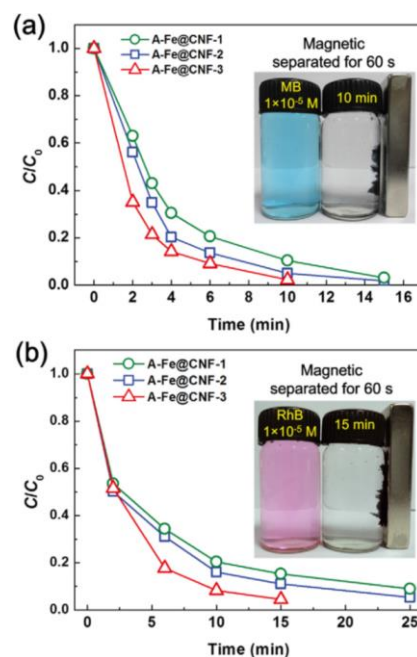

Fig. 18. The C/C0 versus time plots for adsorption of (a) MB and (b) RhB dye solution. The insets show the magnetic responsive performance (60 s) of A-Fe@CNF-3 after adsorption of MB (10 min) and RhB (15 min) [112].

Hierarchical porous, magnetic Fe_3O_4@CNFs parade effective adsorption for organic dyes in water and good magnetic separation performance. Fig. 18 exhibits the pertinent adsorption curves. It was found that Fe_3O_4@CNFs exhibited excellent adsorption ability in the removal of MB and RhB dyes [112].

Porous ZnO/SnO_2 nanofibers were created by a simple electrospinning method [120]. All the fibers/tubes were composed of many nanoparticles that made the porous structure. Photodegradation ability of nanofibers in various dye wastewaters were measured, which showed fast photodegradation and good recycling ability [120]. Removal of acidic and direct dyes using polyamide-6/chitosan nanofibrous filter media was investigated in another research [121]. The dye removal efficiency increased with an increase in the electrospinning time, which was more significant for direct dye. In addition, the effect of chitosan ratio was of lower importance for acidic dye than that for direct dye [121].

4) Sensors

H_2S sensing properties of the porous SnO_2 nanofibers were tested and the effect of CuO amount on the response and recovery characteristics to H_2S was studied [69]. It was found that the response is strongly dependent on the CuO content and the response time and recovery time became longer with the increase in the CuO amount [69]. Porous pitch-based CNFs with multi-walled carbon nanotubes (MWCNTs) were fabricated via an electrospinning method and used as gas sensor electrodes [122]. Due to the high porosity and electrical conductivity, gas adsorption sites were distended and electron transfer was enhanced, resulting in a high-performance NO gas sensor with excellent sensitivity and rapid response time [122]. In another work, nafion nanofibers with regularly porous structure were used to advance super-sensitive humidity sensors [62]. Zhang *et al.* showed highly porous SnO_2 nanofibers could exhibit large response to ethanol and low detection limit [61]. Aligned porous PS nanofibers were fabricated under the mechanism of phase separation. The high-specific surface of these nanofibers could improve recovery of the target sulfonamides 4–10 times compared with that of PS nonporous bulk material [123]. Wrinkled and porous ZnO–SnO_2 hollow nanofibers with an average diameter of 150 nm were created. A sensor based on these nanofibers exhibited highly improved ethanol sensing properties at the optimum temperature of 260 °C [124]. Jin Choi *et al.* developed a simple method for controlling both the size and distribution of spherical pores in electrospun WO_3 nanofibers. Porous WO_3 NFs with a maximized pore diameter showed a high response towards large and heavy acetone molecules. Gas sensing characteristics of WO_3 nanofibers are shown in Fig. 19 [125].

In a similar research work, pore-loaded WO_3 nanofibers having nanoneedle branches were successfully synthesized. The unique morphology and structure of WO_3 nanofibers caused enhanced acetone sensing performance [126]. Also, in another work, pore-loaded WO_3 nanofibers functionalized with spherical catalyst films exhibited

significantly developed toluene and acetone detection capability for application in exhaled breath analysis [127].
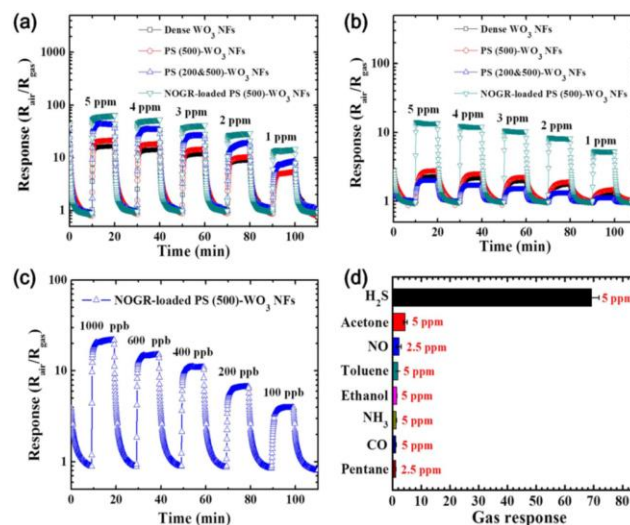

Fig. 19. Gas sensing characteristics of dense WO3 NFs, PS (500)-WO3 NFs, PS (200&500)-WO3 NFs, and PS (500)-WO3 NFs funtionalized with 0.1 wt% non-oxidized graphene (NOGR) flakes in the gas concentration in the range of 1–5 ppm at 350 °C toward (a) H2S and (b) acetone. (c) Limit of detection of the PS (500)-WO3 NFs funtionalized with 0.1 wt% NOGR flakes toward H2S down to 100 ppb at 300 °C. (d) Selective H2S detection characteristic of the PS (500)-WO3 NFs funtionalized with 0.1 wt% NOGR flakes with respect to the interfering analytes at 300 °C [125].

5) Dye-sensitized solar cells

Activated CNFs with hollow core/highly mesoporous shell structure (Meso-HACNF) were prepared with high efficiency of 7.21%. It showed comparability to Pt counter electrode because of its novel characteristics, which promoted the electron and ion transfer, decreased the resistance of charge transfer, and increased the contact area between liquid electrolyte and Meso-HACNF [83]. Porous hollow tin oxide (SnO_2) nanofibers and their composite with TiO_2 particles were examined as a photoanode for dye-sensitized solar cells. Incorporation of TiO_2 particles in porous hollow SnO_2 fibers enhanced the power conversion efficiency [128]. In another study, dyesensitized solar cells were assembled by porous TiO_2 nanofibers that were prepared by electrospinning technique using PVP as template [129]. Dyesensitized solar cells using TiO_2 NFs obtained by 5 wt% of PVP as the photoanode showed higher power conversion efficiency (PCE) of 4.81 % than those obtained by using 8 and 10 wt% of PVP [129].

6) Batteries

The sulfur cathodes fabricated with mesoporous CNFs showed much better electrochemical performance compared with previously reported cathodes. Also, the variation of porous architectures of the carbon framework resulted in very different electrochemistry [71]. Recently, Si-C hybrid nanofibers with a core-shell structure of Si nanoparticles confined in porous CNFs have been designed. The nanofibers displayed good cycling performance and rate capabilities for application as an anode material for lithium-ion batteries (LIBs) [72]. Wang
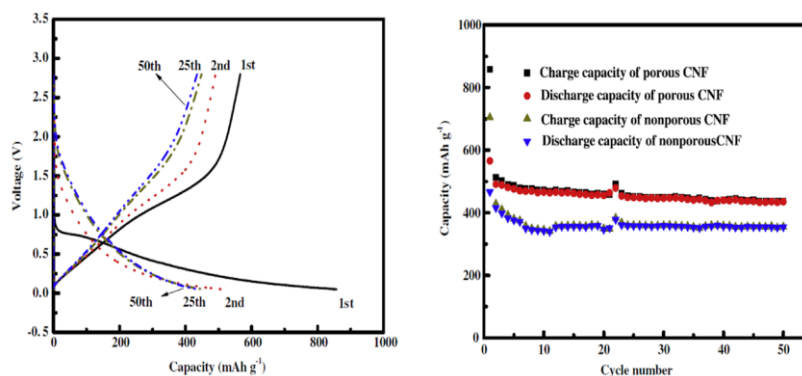
Fig. 20. Charge–discharge curves of porous CNF anode made from PAN/PLLA (9:1) nanofibers at a constant current density of 50 mA g-1 and cycling performance of nonporous and porous CNF anodes made from PAN and PAN/PLLA (9:1) nanofibers, respectively [79].

et al. showed nanoscale porous CNFs could improve lithium-ion storage properties when used as anode material in LIBs [87]. In another similar work, porous CNFs were used as anode for LIBs without any binder or other additives. Compared with the conventional graphite anode, porous CNFs showed high reversible capacity and relatively stable cycle performance (Fig. 20) [79].

It was found that Carbon/Si porous composite nanofibers can be used as anode materials for rechargeable LIBs. These composite nanofibers presented large accessible surface area, high reversible capacity, and relatively good cycling performance at high current densities [80]. The electrodes made of porous $LiNb_3O_8$ nanofibers with interconnected nanocrystals and numerous nanopores presented high capacity, good rate capability, and excellent capacity retention upon cycling, when used as anodes in LIBs [73]. The mesoporous $ZnFe_2O_4$/carbon composite nanofibers exhibited excellent cyclability and rate performance as anodes of LIBs [130]. In order to achieve a high capacity and capacity retention of Ge-based Lithium-ion batteries, porous GeO_2/SnO_2 (GS) nanofibers used as the anode materials of rechargeable LIBs. The excellent properties were due to porous nanostructure which could decrease the transport path and offer a strong retention of electrolyte ions to meet the demands of fast charge and discharge reactions [131]. In a similar work, a high performance long-life Li-ion cell was fabricated using porous α-Fe_2O_3 nanofibers as anode [132]. A new mesoporous carbon/silicon composite nanofiber mats were tested as anode material for lithium ion batteries and exhibited larger lithium capacity and better cycling stability when compared with the nonporous C/Si composite nanofibers as the LIBs anode [133]. Electrochemical properties of porous core/dense shell α-Fe_2O_3 nanofibers were investigated in another study. The initial charge and discharge capacities, rate and cycling performances of the α-Fe_2O_3 nanofibers with a porous core/dense shell structure were higher than those of the nanofibers with other morphologies [134]. The flexible PCNF@MoS_2 composite membrane electrode revealed improvement in electrochemical performance with a high specific capacity, a high rate capability and good cycling stability, indicating its potential application for lithium-ion batteries [135]. In another study, electrochemical measurements showed that PCNFs/S nanocomposite can deliver 400 and 340 mA h g^{-1} after 50 cycles and 100 cycles at 0.5 C, corresponding to 80.1% and 68% capacity retention with a high Coulombic efficiency, respectively [136]. A flexible and highly porous carbon nanofibers (HPCNFs) anode for LIBs showed significant lithium ion storage properties with a good capacity and cycling stability. Schematic illustration of a flexible lithium-ion battery assembled using HPCNFs film as the anode is presented in Fig. 21 [137].
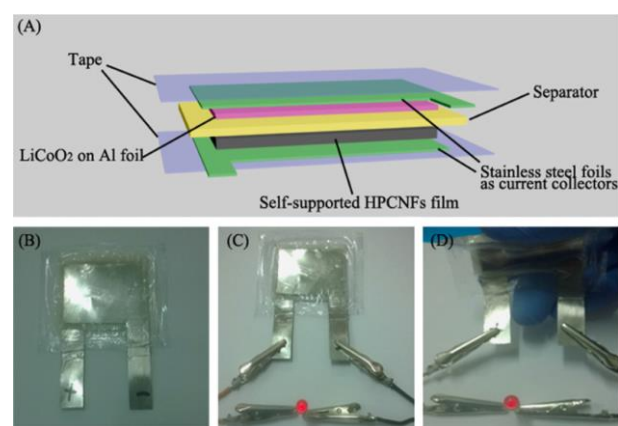

Fig. 21. (A) Schematic illustration of a flexible lithium-ion battery assembled using HPCNFs film as the anode and commercial $LiCoO_2$ loaded on Al foil as the cathode; (B–D) digital photographs of a flexible battery (B) and a red LED lightened by the flexible battery under flat (C) and bent (D) states [137].

Porous nickel oxide (NiO) nanofibers were employed as electrode materials in supercapacitors and lithium-ion batteries. The results showed that after being applied as anode materials in lithium-ion batteries, the nanofibers showed reversible capacity of ~600 mAh g^{-1} after 100 cycles at 1 C rate [138].

7) Energy storage

Two types of porous CNFs, i.e., mesoporous CNFs as electrode materials for supercapacitors, and microporous CNFs as substrate media for lithium–sulfur (Li-S) batteries were reported [139]. The supercapacitor electrodes showed a rescindable specific capacitance and the Li-S batteries

composed of microporous carbon nanofiber exhibited extraordinary electrochemical performance with high specific capacity and good cycling stability [139]. Lately, carbon-coated Li_3N porous nanofibers were produced by a single-nozzle electrospinning system which exposed significantly superior hydrogen storage properties [84]. In another research, highly porous CNFs-supported nickel nanoparticles were prepared as a capable material for hydrogen storage [140]. A study on activated porous CNFs with KOH and $ZnCl_2$ revealed that specific surface area and total pore volume were important factors for increasing the capacity of hydrogen adsorption [88].

8) Catalysts

The photocatalytic activity of the ribbon-like porous nanofibers, ultrafine nanofibers, $LaFeO_3$ powders and TiO_2 was investigated by the degradation of MB in an aqueous solution. The results show that the porous nanofibers exhibit excellent photocatalytic activity compared with ultrafine $LaFeO_3$ nanofibers and $LaFeO_3$ powders [77]. Porous iron–nitrogen–carbon (Fe–N–C) nanofibers were synthesized as metal catalysts to investigate the impact of surface area on electrocatalysis performance. The surface area was controlled by modifying the proportion of the added Si nanoparticles, which showed the development of the electrocatalysis performance [141]. Photocatalytic activity of large-pore mesoporous ZnO nanofibers (Fig. 22) for the hydrogen evolution under the splitting water of the as-fabricated products showed that the porous nanofibers had higher photocatalytic activity than conventional solid nanofibers [142].
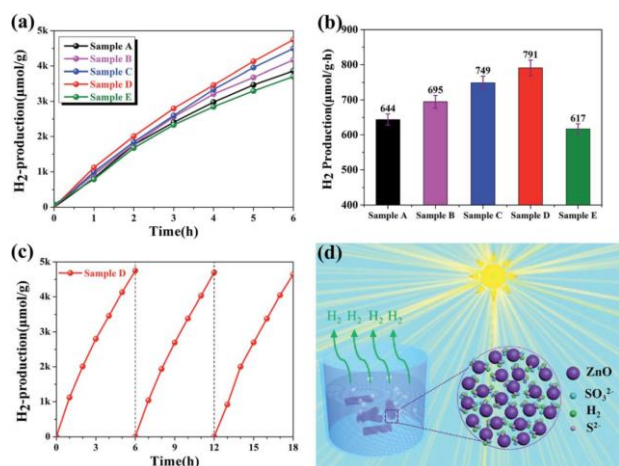

Fig. 22. (a) Photocatalytic hydrogen production rate for Samples A (0 wt %), B (4 wt %), C (5 wt %), D (6 wt %) and E (7 wt %) of foaming agent. (b) Comparison of the photocatalytic activity of Samples A, B, C, D and E during H_2 production. (c) Time course photocatalytic hydrogen evolution for Sample D. (d) A schematic illustration of the large-pore mesoporous nanofibers with enhanced photocatalytic activities [142].

In a recent study, the hierarchically porous structure of the Ceria (CeO_2) nanofibers allowed the facile deposition of Pt nanoparticles via heterogeneous nucleation in a photochemical method. The high porosity of CeO_2 nanofibers and the uniform distribution of Pt nanoparticles enhanced the activity and stability of this catalytic system toward the water-gas shift reaction [143].

9) Superhydrophobic surfaces

Through the surface modification of the porous silica nanofibers with fluorinated silane coupling agents, superhydrophobic surfaces with large contact angle and low sliding angle were fabricated [76]. The superhydrophobic surfaces from silica nanofiber films are of practical significance for various applications including self-cleaning surfaces, antifouling coatings, coatings for microfluidic channels and biosensors, and so on [76]. In another research work, porous structures of silica nanofiber membranes were demonstrated to be effective to achieve superhydrophobic surface after the fluoroalkylsilane (FAS) monolayer modification [47].

10) Other various applications

Mesoporous CNFs show high gas sorption property, which interestingly presents the *p*-type semiconducting behavior [58]. Pt catalysts supported on porous CNFs were created by a co-electrospinning shadowed by a reduction method, for upgraded methanol oxidation in direct methanol fuel cells (DMFCs) in the work of Ahn *et al.* [78]. Pt catalysts supported on porous CNFs exhibit the highest electrocatalytic activity and superior electrocatalytic stability as compared to Pt/conventional CNFs [78]. Microporous CNFs from biomass tar/PAN/silver hybrids with antimicrobial competences were invented. Silver nitrate was reduced to silver nanoparticles, which considered the antimicrobial aptitudes to the CNFs. Antimicrobial activities of the as-spun nanofibers and CNFs with different tar contents against *S. aureus* are demonstrated in Fig. 23 [144].
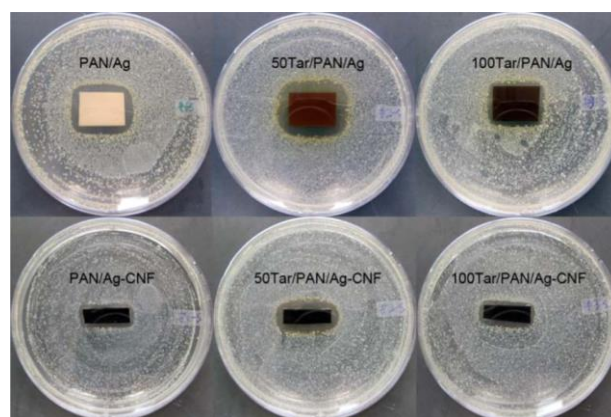

Fig. 23. Antimicrobial activities of the as-spun nanofibers (upper row) and CNFs (lower row) with different tar contents against *S.aureus* [144].

Cellulose acetate (CA) nanofibers in different diameters and different layer thickness were used as a nanofibrous cigarette filters. Tar removal efficiency improved by increasing the unit area weight of filter media [145]. Electrospun polyamide-66 nanofiber layer was fabricated for high-performance nanofiltration in clean room applications. Results of this study show that air permeability decreased and overall filtration efficiency of the produced layer was improved by increasing the coating time [146]. The effect of surface porosity and nanofibers excellence was considered as the main factors of wicking in fibrous PLLA yarn structure [103]. Experimental

indications exposed that surface porosity and fineness of nanofibers have a dominant effect on the capillary rise phenomenon. Changing the surface porosity showed more pronounced effects in wicking height. The results confirmed that finer nanofibers and smooth surface would be more beneficial for wicking in porous PLLA nanofiber yarns [103].

II. CONCLUSION

In recent few years, porous nanofibers with their ultra-fine diameter, high specific surface area, and abundant pores represent an original class of porous materials are used widely in a wide range of applications. Through this review, various concepts for constructing and characterization of porous nanofibers were pronounced. In addition, some instances of porous nanofiber application aptitudes were revealed.

Generally, selective dissolution technique, selective pyrolyzate composite formation, phase separation and breath figure during electrospun process were presented in many research works as the most commonly used procedures for fabrication of porous nanofibers. In selective dissolution and selective pyrolyzate procedures, one component such as a polymer, nanoparticles or other additives was removed during elctrospinning and the process was followed by an after treatment process which led to the porous structure. Porous nanofibers could be obtained by phase separation and breath figure mechanisms when the jet moves from syringe to collector during electrospinning process. In fact, pore creation occurs by decreasing temperature, loss of solvent, or increase in nonsolvent (moisture) throughout these two methods. TIPS and VIPS are most relevant phase separation mechanisms through porous nanofibers formation. During TIPS, phase separation occurs by lowering the temperature of the solution as the fluid jets traverse between the nozzle and the collector. The VIPS method includes the penetration of a nonsolvent vapor causing phase separation of the polymer solution.

Microscopic investigations were used in various research works to study the nanofibers porosity. According to these studies, SEM was used usually for analysis of surface porosity and TEM was applied to consider inner porous structure of nanofibers. Although, determining of porosity percentage was reported using AFM, it was used mostly for measuring depth and diameter of pores. Moreover, the use of the BET technique for estimation of nanofibers surface area and porosity has been reported extensively. Application of BET method in many studies around nanofibers porosity represented useful information such as specific surface area, total pore volume, average pore size and average pore width.

The results of numerous studies indicate that porous nanofibers revealed exceptional potential for a variety of applications. Ultra-fine diameter and porous structure in the electrospun porous nanofibers lead to unique valuable properties that are suitable for wide application expanses such as medical usages, adsorption/separation materials, catalysts, supercapacitors, energy storage, sensors, superhydrophobic materials, batteries, conductors, fuel cells, dye-sensitized solar cells, and filtration.

In conclusion, considering the recent research works, it could be deduced that achieving engineered pore size and pore distribution on the outer and inner structure of nanofibers is a challenging investigation that needs further studies. Also, there is a lack of knowledge in the initiation of porosity on variety of polymeric nanofibers which impose a limitation on their potential applications. Advances in this field could lead to more exclusive properties and other different application capacities of porous nanofibers.

REFERENCES

[1] S. Ramakrishna, K. Fujihara, W. E. Teo, T. C. Lim, and Z. Ma, An introduction to electrospinning and nanofibers, Singapore: World Scientific, 2005.

[2] M. F. Ashby, P. J. Ferreira, and D. L. Schodek, Nanomaterials, nanotechnologies and design, USA : Elsevier, 2009.

[3] Y. S. Lee and J. S. Im, Preparation of functionalized nanofibers and their applications; Nanofibers, Ashok Kumar (Ed.), ISBN: 978-953-7619-86-2, InTech, Available from: http://www.intechopen.com/books/nanofibers/preparation-of-functionalized nanofibers-and-their-applications.

[4] M. U. Niemann, S. S. Srinivasan, A. R. Phani, A. Kumar, D. Y. Goswami, E. K. Stefanakos, "Nanomaterials for hydrogen storage applications: a review", *J Nanomater.*, (2008) doi:10.1155/2008/950967.

[5] A. L. Andrady, Science and technology of polymer nanofibers, USA: Wiley, 2008.

[6] R. Khajavi and M. Abbasipour, "Electrospinning as a versatile method for fabricating coreshell, hollow and porous nanofibers", *Scientia Iranica F.,* vol. 19, pp. 2029, 2012.

[7] M. S. Esfandarani and M. S. Johari, Producing porous nanofibers, Nanocon 2010, Czech Republic, 12 October2010 - 14 October2010.

[8] M. N. Shuakat and T. Lin, "Recent Developments in Electrospinning of Nanofiber Yarns", *J. Nanosci. Nanotechnol.,* vol. 14, pp. 1389, 2014.

[9] Y. Zhang, C. T. Lim, S. Ramkarishna, and Z. M. Huang, "Recent development of polymer nanofibers for biomedical and biotechnological applications", *J. Mater. Sci. - Mater. Med.,* vol. 16, pp. 933, 2005.

[10] W. E. Teo and S. Ramakrishna, "A reviewon electrospinning design and nanofibre assemblies", *Nanotechnology.,* vol. 17, pp. R89, 2006.

[11] S. K. Smoukov, T. Tian, N. Vitchuli, S. Gangwal, P. Geisen, M. Wright, E. Shim, M. Marquez, J. Fowler, and O. D. Velev, "Scalable liquid shear-driven fabrication of polymer nanofibers", *Adv. Mater.,* vol. 27, pp. 2642, 2015.

[12] R. Chen, Y. Li, and J. He, "Bubbfil spinning for mass-production of nanofibers", *Therm. Sci.,* vol. 18, pp. 1718, 2014.

[13] R. Chen, Y. Li, and J. He, "Mini-review on bubbfil spinning process for mass-production of nanofibers", *Matéria.,* vol. 19, pp. 325, 2014.

[14] C. Ning, C. He, L. Xu, F. Liu, and J. He, "Nano-dyeing", *Therm. Sci.,* vol. 20, pp. 1003, 2016.

[15] C. Liu, L. Zhao, X. Li, and J. He, "Hierarchical structure of nanofibers by bubbfil spinning", *Therm. Sci.,* vol. 19, pp. 1445, 2015.

[16] Y. Li, J. He, Q. Sun, and P. Wang, "High temperature resistant nanofiber by bubbfil-spinning", *Therm. Sci.,* vol. 19, pp. 1461, 2015.

[17] Y. Zhao, Y. Qiu, H. Wang, Y. Chen, S. Jin, and S. Chen, "Preparation of nanofibers with renewable polymers and their application in wound dressing", *International Journal of Polymer Science*., 2016.

[18] J. Shen, C. He, H. Liu, and L. Zhao, "Effect of pore size on gas resistance of nanofiber membrane by the bubble electrospinning", *Therm. Sci*., vol. 19, pp. 1349, 2015.

[19] C. Burger, B. S. Hsiao, and B. Chu, "Nanofibrous materials and their applications", *Annu. Rev. Mater. Res.,* vol. 36, pp. 333, 2006.

[20] S. Ramakrishna, K. Fujihara, W. E. Teo, T. Yong, Z. Ma, and R. Ramaseshan, "Electrospun nanofibers: solving global issues", *Mater. Today*., vol. 9, pp. 40, 2006.

[21] K. Yoon, B. S. Hsiao, and B. Chu, "Functional nanofibers for environmental applications", *J. Mater. Chem.,* vol. 18, pp. 5326, 2008.

[22] X. Lu, C. Wang, and Y. Wei, "One-dimensional composite nanomaterials: synthesis by electrospinning and their applications", *Small.,* vol. 5, pp. 2349, 2009.

[23] J. Xie, M. R. Macewan, A. G. Schwartz, and Y. Xia, "Electrospun nanofibers for neural tissue engineering", *Nanoscale.,* vol. 2, pp. 35, 2010.

[24] C. L. Casper, J. S. Stephens, N. G. Tassi, D. B. Chase, and J. F. Rabolt, "Controlling surface morphology of electrospun polystyrene fibers: effect of humidity and molecular weight in the electrospinning process", *Macromolecules.,* vol. 37, pp. 573, 2004.

[25] A. Greiner and J. H. Wendorff, "Electrospinning: a fascinating method for the preparation of ultrathin fibers", *Angew. Chem. Int. Ed.,* vol. 46, pp. 5670, 2007.

[26] J. Lin, X. Wang, B. Ding, J. Yu, G. Sun, and M. Wang, "Biomimicry via electrospinning", *Crit. Rev. Solid State Mater. Sci.,* vol. 37, pp. 94, 2012.

[27] C. H. Kim, Y. H. Jung, H. Y. Kim, D. R. Lee, N. Dharmaraj, and K. E. Choi, "Effect of collector temperature on the porous structure of electrospun fibers", *Macromol. Res.,* vol. 14, pp. 59, 2006.

[28] D. H. Reneker, and I. Chun, "Nanometre diameter fibres of polymer, produced by electrospinning", *Nanotechnology*., vol. 7, pp. 216, 1996.

[29] T. Subbiah, G. S. Bhat, R. W. Tock, S. Parameswaran, and S. S. Ramkumar, "Electrospinning of nanofibers", *J. Appl. Polym. Sci.,* vol. 96, pp. 557, 2005.

[30] S. Koombhongse, W. Liu, and D. H. Renker, "Flat polymer ribbons and other shapes by electrospinning", *J. Polym. Sci., Part B: Polym. Phys.,* vol. 39, pp. 2598, 2001.

[31] M. M. Hohman, M. Shin, G. Rutledge, and M. P. Brennera, "Electrospinning and electrically forced jets", II. Applications. *Phys. Fluids.,* vol. 13, pp. 2221, 2001.

[32] V. Pillay, C. Dott, Y. E. Choonara, C. Tyagi, L. Tomar, P. Kumar, L. C. du Toit, and V. M. K. Ndesendo, "A review of the effect of processing variables on the fabrication of electrospun nanofibers for drug delivery applications", *J Nanomater,*. doi:10.1155/2013/789289, 2013.

[33] A. Rabbi, K. Nasouri, H. Bahrambeygi, A. M. Shoushtari, and M. R. Babaei, "RSM and ANN approaches for modeling and optimizing of electrospun polyurethane nanofibers morphology", *Fiber Polym.,* vol. 13, pp. 1007, 2012.

[34] X. H. Qin, E. L. Yang, N. Li, and S. Y. Wang, "Effect of different salts on electrospinning of polyacrylonitrile (PAN) polymer solution", *J. Appl. Polym. Sci.,* vol. 103, pp. 3865 ,2007.

[35] M. M. Demir, I. Yilgor, E. Yilgor, and B. Erman, "Electrospinning of polyurethane fibers", *Polym. J.,* vol. 43, pp. 3303, 2002.

[36] K. Nasouri, H. Bahrambeygi, A. Rabbi, A. M. Shoushtari, and A. Kaflou, "Modeling and optimization of electrospun PAN

[37] nanofiber diameter using response surface methodology and artificial neural networks", *J. Appl. Polym. Sci.,* vol. 126, pp. 127, 2012.

[37] S. O. Han, W. K. Son, D. Cho, J. H. Youk, and W. H. Park, "Preparation of porous ultra-fine fibres via selective thermal degradation of electrospun polyetherimide/poly(3-hydroxybutyrate-co-3-hydroxyvalerate) fibres", *Polym. Degrad. Stab. Stability.,* vol. 86, pp. 257, 2004.

[38] M. Ziabari, V. Mottaghitalab, and A. Khodaparast Haghi, "Evaluation of electrospun nanofiber pore structure parameters", *Korean J. Chem. Eng.,* vol. 25, pp. 923, 2008.

[39] K. Ishizaki, S. Komarneni, and M. Nanko, Porous Materials: Process technology and applications. USA: Springer Science+Business Media Dordrecht, 1998.

[40] M. Peng, D. Li, L. Shen, Y. Chen, Q. Zheng, and H. Wang, "Nanoporous structured submicrometer carbon fibers prepared via solution electrospinning of polymer blends", *Langmuir.,* vol. 22, pp. 9368, 2006.

[41] S. B. Jenkins: Nanoporous materials, types, properties and uses. New York: Nova Science Publishers, 2010.

[42] J. H. He, Y. Liu, L. Xu, and J. Y. Yu, "Micro sphere with nanoporosity by electrospinning", *Chaos Solitons Fractals.,* vol. 32, pp. 1096, 2007.

[43] S. Ernst: Advances in nanoporous materials. Netherlands: Elsevier, 2009.

[44] Y. Z. Zhang, Y. Feng, Z. M. Huang, S. Ramakrishna, and C. T. Lim, "Fabrication of porous electrospun nanofibers", *Nanotechnology*., vol. 17, pp. 901, 2006.

[45] Y. Qiu, J. Yu, X. Zhou, C. Tan, and J. Yin, "Synthesis of porous NiO and ZnO submicro- and nanofibers from electrospun polymer fiber templates", *Nanoscale Res. Lett.,* vol. 4, pp. 173, 2009.

[46] S. C. Moon, J. K. Choi, and R. J. Farris, "Highly porous polyacrylonitrile/polystyrene nanofibers by electrospinning", *Fiber Polym.,* vol. 9, pp. 276, 2008.

[47] M. Kanehata, B. Ding, and S. Shiratori, "Nanoporous ultra-high specific surface inorganic fibres", *Nanotechnology.,* vol. 18, pp. 3156021, 2007.

[48] H. Chen, J. Di, N. Wang, H. Dong, J. Wu, Y. Zhao, J. Yu, and L. Jiang, "Fabrication of hierarchically porous inorganic nanofibers by a general microemulsion electrospinning approach", *Small.,* vol. 7, pp. 1779, 2011.

[49] M. Teng, J. Qiao, F. Li, and P. K. Bera, "Electrospun mesoporous carbon nanofibers produced from phenolic resin and their use in the adsorption of large dye molecules", *Carbon.,* vol. 50, pp. 2877, 2012.

[50] L. Ji, A. J. Medford, and X. Zhang, "Porous carbon nanofibers loaded with manganese oxide particles: Formation mechanism and electrochemical performance as energy-storage materials", *J. Mater. Chem.,* vol. 19, pp. 5593 ,2009.

[51] Z. Zhang, X. Li, C. Wang, S. Fu, Y. Liu, and C. Shao, "Polyacrylonitrile and carbon nanofibers with controllable nanoporous structures by electrospinning", *Macromol. Mater. Eng.,* vol. 294, pp. 673, 2009.

[52] D. Lubasova and L. Martinova, "Controlled morphology of porous polyvinyl butyral nanofibers", *J Nanomater.,* doi:10.1155/2011/292516, 2011.

[53] G. Ma, D. Yang, and J. Nie, "Preparation of porous ultrafine polyacrylonitrile (PAN) fibers by electrospinning", *Polym. Adv. Technol.,* vol. 20, pp. 147, 2009.

[54] L. Ji, C. Saquing, S. A. Khan, and X. Zhang, "Preparation and characterization of silica nanoparticulate–polyacrylonitrile composite and porous nanofibers", *Nanotechnology*., vol. 19, pp. 0856051, 2008.

[55] A. Gupta, C. D. Saquing, M. Afshari, A. E. Tonelli, S. A. Khan, and R. Kotek, "Porous nylon-6 fibers via a novel salt-induced electrospinning method", *Macromol.,* vol. 42, pp. 709,